coatings

MDPI

Article

Influence of Graphite and Zirconia Addition on the Tribological Properties of Plasma-Sprayed Alumina Coatings

Liutauras Marcinauskas [1,2,*], Karina Ratautaitė [1,2], Žydrūnas Kavaliauskas [1], Audrius Žunda [3], Romualdas Kėželis [1] and Mindaugas Aikas [1]

[1] Plasma Processing Laboratory, Lithuanian Energy Institute, Breslaujos Str. 3, LT-44403 Kaunas, Lithuania; karina.ratautaite@ktu.edu (K.R.); zydrunas.kavaliauskas@lei.lt (Ž.K.); romualdas.kezelis@lei.lt (R.K.); mindaugas.aikas@lei.lt (M.A.)
[2] Department of Physics, Kaunas University of Technology, Studentu Str. 50, LT-51368 Kaunas, Lithuania
[3] Department of Mechanical, Energy and Biotechnology Engineering, Faculty of Engineering, Vytautas Magnus University Agriculture Academy, LT-53361 Kaunas, Lithuania; audrius.zunda@vdu.lt
* Correspondence: liutauras.marcinauskas@ktu.lt

Abstract: Al_2O_3, Al_2O_3-graphite and Al_2O_3-ZrO_2 coatings were formed on the C45 steel rolls using atmospheric plasma spraying. The influence of graphite and zirconia addition on the surface morphology, phase composition and tribological properties under dry sliding conditions using 30 N load were analyzed. It was found that the addition of graphite or ZrO_2 slightly affected the fraction of the α-Al_2O_3 and γ-Al_2O_3 phases in the alumina coatings. The highest mass loss rate (~8.84×10^{-4} g/s) was obtained for the friction pair of C45 steel roll and steel plate. The friction coefficient of the Al_2O_3-graphite coating was slightly lower (up to 7%) compared to the coating of Al_2O_3-ZrO_2. However, the friction pair of Al_2O_3-ZrO_2 coating and steel plate demonstrated the highest wear resistance under dry sliding conditions. The increase in the wear resistance of the Al_2O_3-graphite and Al_2O_3-ZrO_2 coatings is due to the formation of tribofilm in the sliding contact zone.

Keywords: alumina-graphite; alumina-zirconia; coatings; plasma spraying; tribology; friction coefficient

Citation: Marcinauskas, L.; Ratautaitė, K.; Kavaliauskas, Ž.; Žunda, A.; Kėželis, R.; Aikas, M. Influence of Graphite and Zirconia Addition on the Tribological Properties of Plasma-Sprayed Alumina Coatings. *Coatings* **2024**, *14*, 978. https://doi.org/10.3390/coatings14080978

Academic Editor: Jose Luis Viesca

Received: 31 May 2024
Revised: 19 July 2024
Accepted: 26 July 2024
Published: 2 August 2024

1. Introduction

Aluminum oxide coatings are widely used due to their low electrical conductivity, high resistance to thermal degradation and corrosion impact, excellent mechanical and tribological properties. Because of these versatile properties, Al_2O_3 coatings are widely used to protect metal surfaces from corrosion or wear in order to extend the service life of metal parts [1–6]. However, despite their high hardness and relatively low friction coefficient in a lubricated environment, the friction coefficients of Al_2O_3 coatings under dry sliding conditions are relatively high. In addition, the low fracture toughness and low-fracture strength of alumina also limit its use in structural and tribological applications. It was demonstrated that the toughness and brittleness tribological properties of Al_2O_3 coatings are improved when additives such as TiO_2 [4,7–9], ZrO_2 [8,10–14], CeO_2 [15], graphite [16–19], and graphene nanoplatelets [20–25] or graphene oxide [26–28] are used.

S. Mehar et al. [11] demonstrated that the addition of yttria-stabilized zirconia with various content into Al_2O_3-3 wt.% TiO_2 coating reduced the friction coefficients (up to 65%) and wear rates (up to two times). Additionally, the tribological properties of composite coatings are strongly dependent on the applied loads and sliding velocities. J.J. Kang et al. [7] demonstrated that the phase structures and properties of the Al_2O_3-40 TiO_2 coatings strongly depend on the process parameters. The variation in the TiO_2 content in the Al_2O_3 coatings allows for the improvement of the adhesion strength and for the control of thermal conductivity values [8]. H. Aghajani et al. [2] observed that the addition of 20 wt.% Y_2O_3 increased the alpha Al_2O_3 phase

content from 20% to 32% and reduced the wear rates (up to four times) of the alumina coatings. Y. Chen et al. [12] reported that the increase in the ZrO_2 fraction in the Al_2O_3 coatings reduced the hardness (by 14%) and improved the toughness of the coatings. O. Tingaud et al. [14] observed that the addition of the ZrO_2 doped with 8 wt.% of yttria enhanced the friction coefficient by 5%, but reduced the specific wear rates by more than nine times that of alumina coatings. Y. Wang et al. [16] indicated that the friction coefficient of the Al_2O_3-ZrO_2 coating was 0.74, when the load of 30 N was used. S. Mahade et al. [23] observed that the friction coefficient of the alumina-graphene coatings was ~0.5, i.e., 36% lower than that of the Al_2O_3 coating. D. Franco et al. [6] determined that the friction coefficient of Al_2O_3 coatings varied from 0.80 to 0.97, depending on the nature of the Al_2O_3 feedstock powders used. Y. Li et al. [27] demonstrated that the alumina-graphene oxide coatings had a 31% decrease in porosity and more than 80% lower wear rate compared to alumina coatings. S. S. Mohapatra et al. [28] found that the graphene oxide additive improved the microstructure, hardness and corrosion resistance of the alumina coatings. A. Mulone et al. [22] showed that graphene improves the tribological behavior of alumina coatings. The addition of graphene oxide into the Al_2O_3-CeO_2 coatings improved the hardness and reduced the friction coefficient [29]. The addition of the graphene into Al_2O_3-TiO_2 coatings enhanced the gamma Al_2O_3 phase content and reduced the friction coefficient and the wear rate due to the formation of self-lubricate layer at the contact zone [21]. The addition of CeO_2 resulted in the transformation of γ-Al_2O_3 to α-Al_2O_3 phase in Al_2O_3-TiO_2 coatings [30]. Our previous studies [17–20] indicated that the addition of graphite into alumina resulted in structural changes, reduced the friction coefficient, and enhanced the wear resistance of the alumina-graphite coatings under dry sliding conditions when low loads (up to 3 N) were used. However, the tribological properties of the alumina-graphite coatings strongly depended on the type of graphite used, its initial concentration in the Al_2O_3 feedstock powders and the spraying parameters [17–19]. Several authors [2,3,11] have shown that the friction coefficient and wear rates of ceramic coatings are highly dependent on the loads applied during the tribological tests. The increase in the load from 2 N to 20 N enhanced the weight loss of alumina coatings by a factor of 9 [2]. The enhancement of the load from 12 N to 48 N led to a double increase in the friction coefficient for Al_2O_3 and Al_2O_3-ZrO_2 coatings, respectively [11].

It should be mentioned that the phase structure and the final properties of the Al_2O_3 composite coatings are highly dependent on the type of used additives and their concentrations, the plasma spraying equipment and process parameters used, and the type and size of the feedstock Al_2O_3 powders [4,6–8,17–26]. A review of the literature results shows that even a slight variation in the spraying parameters, the friction evaluation method used or even the applied load can have a significant effect on the tribological properties of alumina coatings.

The main aim of this work was to deposit the Al_2O_3, Al_2O_3-graphite and Al_2O_3-ZrO_2 coatings and to investigate the influence of the graphite and zirconia additives on the structure and tribological behavior of the Al_2O_3 composite coatings under dry sliding at 30 N loads using the coated C45 steel rolls and steel plates as a friction pair.

2. Materials and Methods

The plasma torch used for the deposition of the ceramic coatings was developed at the Lithuanian Energy Institute; more details are given in ref [31]. The coatings were formed on a C45-grade steel roll with an outer diameter of 35 ± 0.2 mm and a width of 12 ± 0.2 mm (Figure 1). The composition of the C45-grade steel is given in Table 1. The steel contained mainly iron, with a low amount of various elements such as C, Mn, Si, Cr, etc. (Table 1).

Table 1. Composition of the C45-grade steel.

C, %	Mn, %	Si, %	Cu, %	Cr, %	Ni, %	Mo, %	P, %	S, %
0.42–0.5	0.5–0.8	0.1–0.4	≤0.3	≤0.3	≤0.3	≤0.1	≤0.04	≤0.04

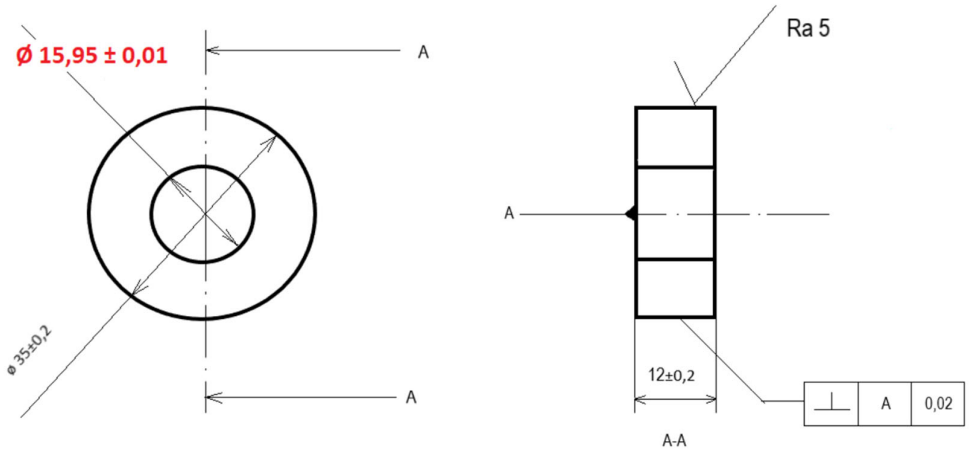

Figure 1. C45 steel roll used for the deposition of the coatings.

The substrates were placed on the holder, which was rotated during the plasma spraying. The plasma torch was moving forward and backward during the deposition. The aluminum bonding layer was sprayed on the C45 steel roll substrate before the deposition of the coatings. The deposition time of all coatings was kept for 60 s, distance from the torch nozzle exit to substrate was 70 mm. The arc current was 180 A and the torch power was 36.0 ÷ 36.4 kW. Air was used as plasma-forming gas (3.75 g/s) and powder-carrier gas (0.75 g/s). Additionally, hydrogen was used to enhance the plasma jet temperature. The spraying parameters were chosen based on our previous investigations [17–19]. The coatings were sprayed using Al_2O_3 (type ALO-101, non-regular shape, size ~45 µm, Praxair Surface Technologies, Indianapolis, IN, USA), graphite (MOLYDUVAL Fondra NS, size < 25 µm (90%), size < 10 µm (10%)) and ZrO_2-8%Y_2O_3 (type ZRO-113/114, 99% purity, spherical shape, PRAXAIR Surface Technologies, Indianapolis, IN, USA) powders. The graphite and zirconium oxide powders were added into the Al_2O_3 feedstock at a weight ratio of 10% to produce Al_2O_3-graphite and Al_2O_3-ZrO_2 powders. The mixtures of alumina-graphite and alumina-zirconia powders were mechanically mixed for 24 h and then dried at ~350 K for at least 18 h before beginning the plasma spray process.

The surface morphology of the ceramic coatings and steel parts before and after tribological tests was investigated using scanning electron microscopy (SEM) with Hitachi S–3400 N (Tokyo, Japan). The roughness measurements of the as-sprayed coatings were measured by stylus profilometer MahrSurf GD 25 (Mahr GmbH, Göttingen, Germany). The roughness values were measured at least 5 times. The energy dispersive X-ray spectroscopy (EDX) (Bruker Quad 5040 spectrometer, AXS Microanalysis GmbH, Hamburg, Germany) was used to measure the elemental composition of the coatings and steel parts before and after the tribological tests. The measurements were performed on a surface area of ~1.15 mm^2 (at 50 magnifications) at 3–5 different points and the average values were obtained. The X-ray diffraction (XRD) (Bruker D8 Discover, Billerica, MA, USA) with a standard Bragg–Brentano, focusing geometry in a 5°–80° range using the CuK_α (λ = 0.154059 nm) radiation, was used to investigate the phase structure of the plasma-sprayed coatings. Tribological tests were performed using the friction-couple roll-on-plate (Figure 2). The roll width was 12 ± 0.2 mm and the diameter was 35 ± 0.2 mm. Plate dimensions: width—12 ± 0.2 mm; length—20 ± 0.2 mm; and thickness—5 ± 0.1 mm. All tribological tests were performed in dry sliding conditions at 21 °C. The tribological pairs of C45 steel roll–C45 steel plate, Al_2O_3 coating–C45 steel, Al_2O_3-graphite coating–C45 steel, and Al_2O_3-zirconia coating–C45 steel were used. The tribological tests were performed using a load of 30 N and the sliding speed was ~3.72 m/s. Maximal shear stress upon contact was 23.1 MPa. The average test duration was 10 min, and the test was stopped at the appearance of an unusual sound in the friction pair, or if a boldly increased coefficient of friction remained for a longer time

(more than 1 min), which actually indicated that the coating was completely worn and adhesive wear between the steel surfaces began. The mass loss of the coatings and counterparts of steel plate was measured using an electronic balance ABJ 120-4M (KERN & Sohn GmbH, Balingen, Germany), the average of the same set samples was calculated, and the mass loss rates were determined.

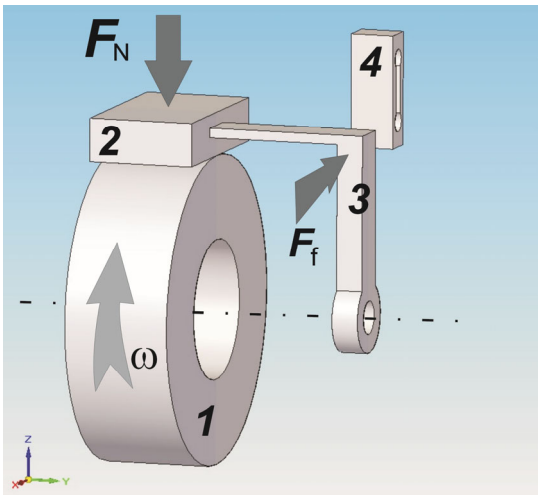

Figure 2. Principal scheme of the roll-on-plate tests used for the determination of the friction coefficient: 1—roller; 2—steel plate; 3—plate holder; 4—force sensor.; F_N—normal force; F_f—friction force; w—rotation speed.

3. Results and Discussion

The morphological views of the deposited Al_2O_3 and Al_2O_3-graphite coatings are given in Figure 3. The surface of the Al_2O_3 coating is homogenous and consists of fully molten splats of 10–30 μm in diameter. Additionally, some partly melted micrometer-sized particles are present (Figure 3).

The addition of the graphite resulted in a slightly improved melting degree of the feedstock particles and lower amount of partly melted particles on the surface of Al_2O_3-graphite coating. It should be mentioned that the spherical or irregularly shaped particles of various sizes ranging from 5 to 20 μm are found on the surface of all as-sprayed coatings (Figure 3c,d). The surface of the Al_2O_3-zirconia coating is composed of the well-melted regions and areas of semi-melted particles (Figure 4). The random distribution of micro-sized pores and voids are found on the surface of Al_2O_3, Al_2O_3-graphite and Al_2O_3-zirconia coatings at higher magnification images (Figures 3 and 4b). The existence of voids and pores on the surface or in the bulk of plasma-sprayed ceramic coatings is a typical phenomenon observed by various researchers [4,7,8,14]. The stacking, spreading and shrinkage process of Al_2O_3 and ZrO_2 droplets stipulates the creation of pores between the particles. Additionally, the randomly distributed microcracks could be observed in all as-sprayed coatings (Figures 3d and 4b). The surface roughness measurements also indicated that the average roughness of the coatings was slightly reduced from ~2.38 μm to ~2.18 μm, when the graphite was used. The surface roughness of the Al_2O_3-zirconia coating was ~2.22 μm.

The EDX results indicated that the concentration of the oxygen and aluminum in the Al_2O_3 coating was 52.0 ± 2.0 wt.% and ~47.5 ± 2.2 wt.%, respectively. It should be mentioned that a low amount (less than 1 wt.%) of impurities related to the nature of used feedstock powder was found. The Al_2O_3-graphite coating consisted of aluminum—50.0 wt.%; oxygen—47.0 wt.%; and graphite—2.3 wt.%. The amount of the aluminum and oxygen in the Al_2O_3-zirconia coating was ~47.4 ± 2.1 wt.% and ~47.8 ± 2.4 wt.%, respectively. The concentration of the zirconium in the Al_2O_3-zirconia coating was ~4.5 wt.%.

The EDX mapping images demonstrated that the graphite was homogeneously distributed on the surface of the coating (Figure 5). The size of the graphite particles on the surface of the coating varied from 2 μm to 10 μm (Figure 5d). The deposition of the coating

with a uniform distribution of graphite particles over the entire surface and volume is very important because the graphite will act as a lubricant in dry friction.

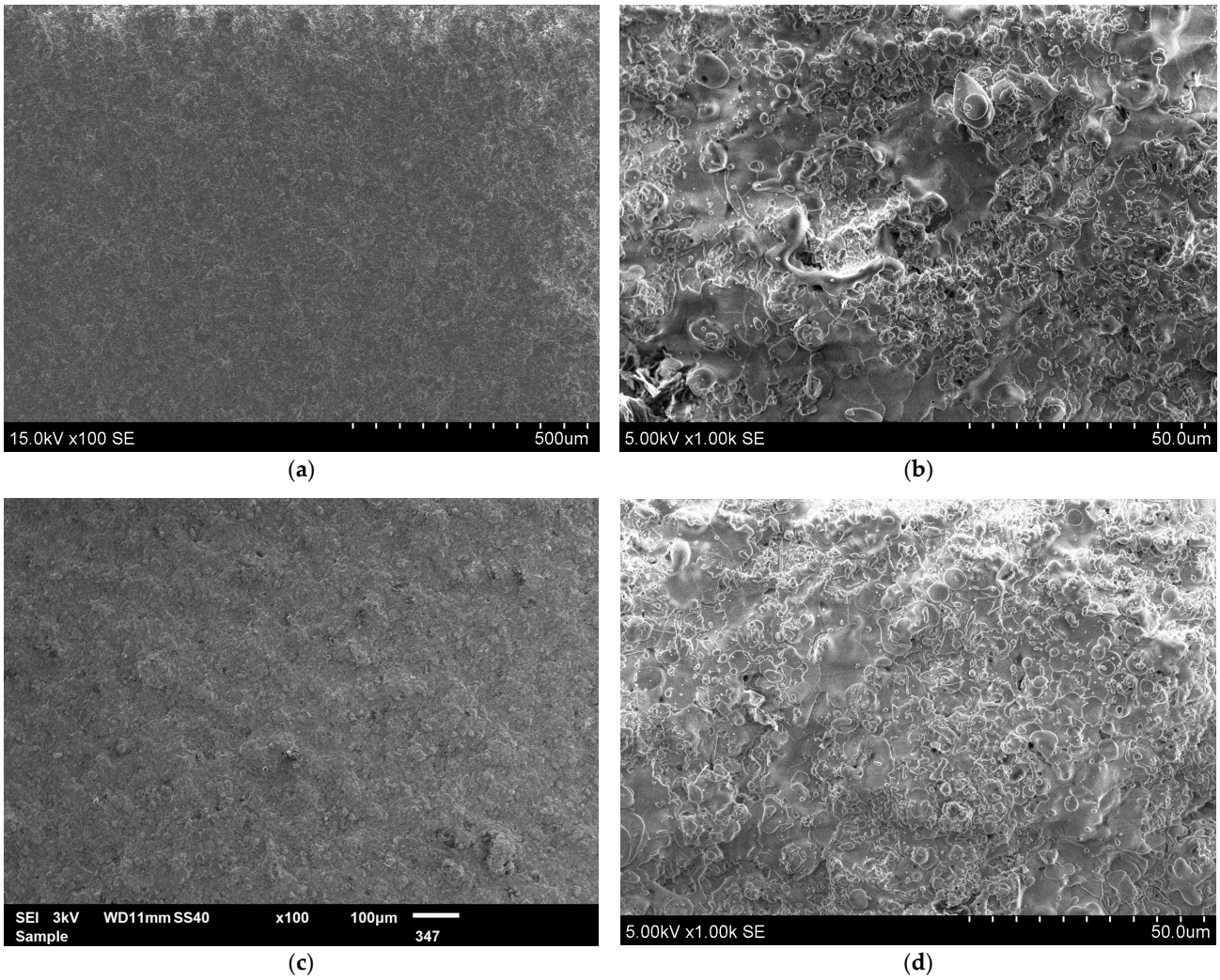

Figure 3. Surface morphology images of the Al_2O_3 (**a**,**b**) and Al_2O_3-graphite (**c**,**d**) coatings.

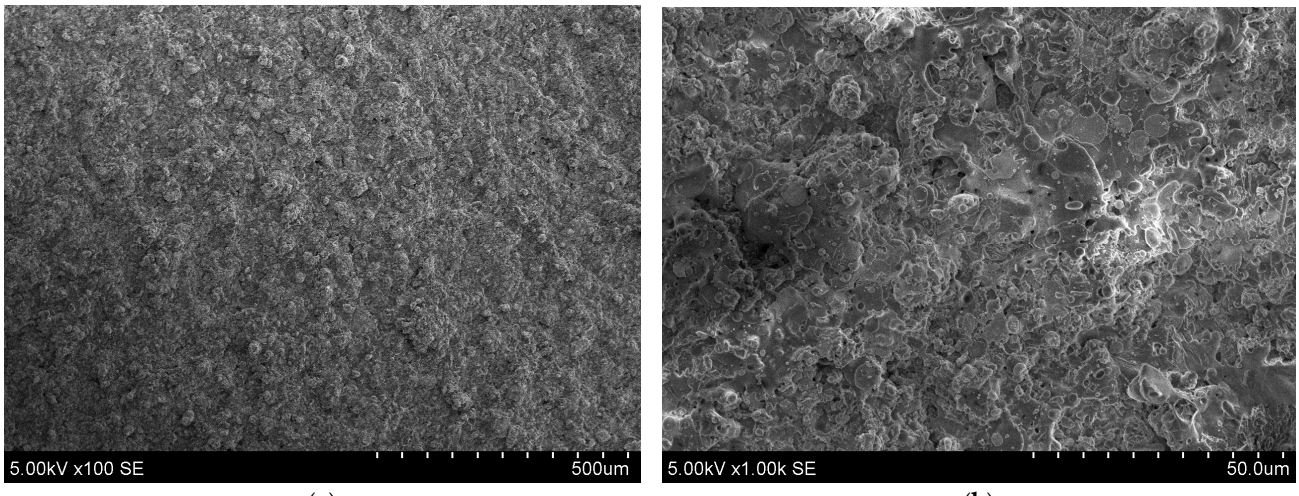

Figure 4. Surface morphology of the Al_2O_3-zirconia coatings. (**a**) 100×, (**b**) 1000× magnification.

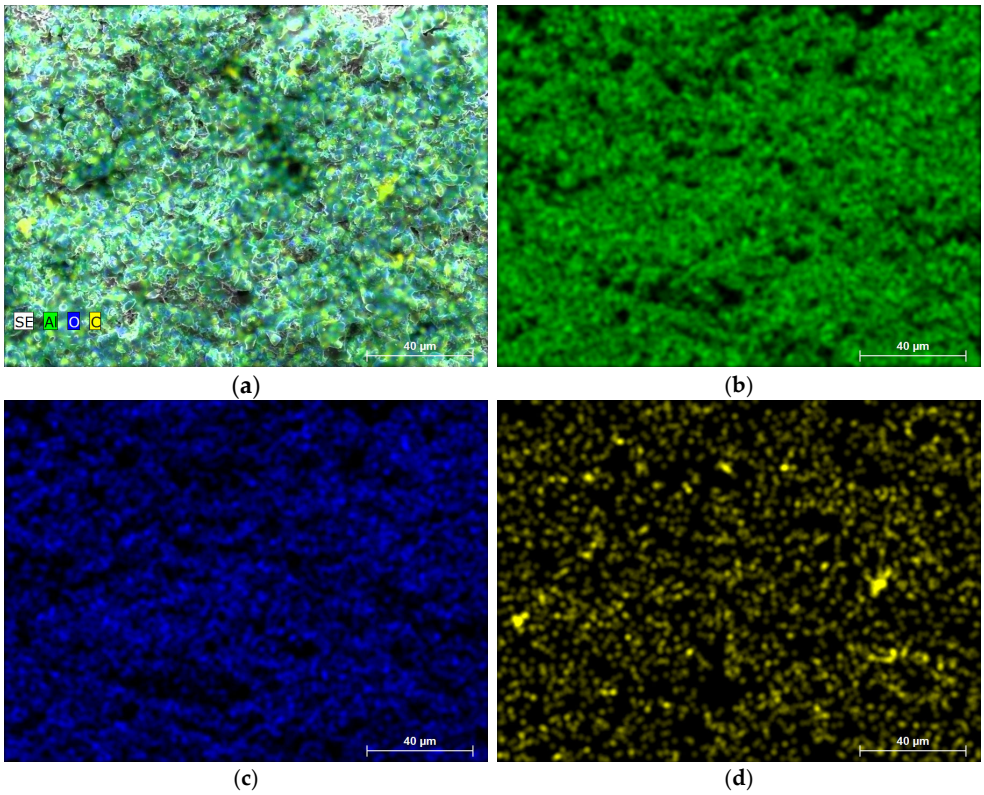

Figure 5. Element mapping images (at 500 magnifications) of as-sprayed Al_2O_3-graphite coating, (**a**) all elements, (**b**) aluminum, (**c**) oxygen and (**d**) carbon.

The XRD patterns of the Al_2O_3, Al_2O_3-graphite and Al_2O_3-zirconia coatings are given in Figure 6. The results indicated that all coatings were composed of α-Al_2O_3 and γ-Al_2O_3 phases. The peaks observed at $2\theta = 25.8^\circ$, 35.4°, 43.6°, 51.4°, 57.8° and 68.2° are attributed to the rhombohedral α-Al_2O_3 phase [2,7,15,20,22,32]. The peaks found at 20.2°, 37.7°, 39.7°, 46.1°, 61.3° and 67.2° are related to the cubic γ-Al_2O_3 phase [2,17,20,22]. The initial alumina powder consisted of a high fraction of the α-Al_2O_3 phase with a low content of the β-Al_2O_3 phase [17]. The peaks obtained at 37.7°, 45.0° and 65.1° are assigned to the aluminum, which was used as bonding layer. The low-intensity peak at 26.5° was observed in the Al_2O_3-graphite coating (Figure 6b). Several authors indicated that this peak is assigned to the crystalline (002) planes of graphite in the ceramic composite coatings [18,33]. It was observed that the intensities of the α-Al_2O_3 and γ-Al_2O_3 phase peaks slightly changed when the graphite or zirconia was added into alumina feedstock powders. In order to determine the phase changes in the coatings, the amount of gamma and alpha phases in Al_2O_3, Al_2O_3-graphite and Al_2O_3-zirconia coatings was evaluated. The volume percent of the alpha-alumina phase in the as-sprayed coatings was calculated using Equation (1) [23]:

$$V_\alpha(\%) = \frac{1}{1 + 1.08\frac{I_{[400]}}{I_{[113]}}} \times 100 \quad (1)$$

where $I_{[113]}$ is the intensity of the (113) peak of α-Al_2O_3 phase (at 43.6°), $I_{[400]}$ is the intensity of the (400) peak of γ-Al_2O_3 phase (at 46.2°), and 1.08 is a correction factor.

The additional peaks at ~28.4°, 30.4°, ~31.6°, 35.3°, 50.5° and 59.9° were obtained for the Al_2O_3-zirconia coatings. The existence of those peaks is related to the zirconium oxide phases in the composite coating [15,34,35]. The peaks located at 30.4°, 35.3°, 50.5° and 59.9° are attributed to the tetragonal ZrO_2 phase of (101), (110), (200) and (211) crystallographic orientations, respectively [34]. The low-intensity peaks obtained at ~28.4° and ~31.6° are due to the monoclinic ZrO_2 phase of (111) and (−111) orientations, respectively [15,34–36].

The monoclinic ZrO_2 phase amount in the coating can be calculated by the methodology given in [34]:

$$C_m = \frac{0.82(I_{m-111} + I_{m111})}{0.82\ (I_{m-111} + I_{m111}) + I_{t101}} \quad (2)$$

where C_m is the content of monoclinic ZrO_2 phase, I is the intensity of diffraction peak in the XRD patterns of the coating (Figure 6c), and the subscripts monoclinic (m) and tetragonal (t) mark the phase type.

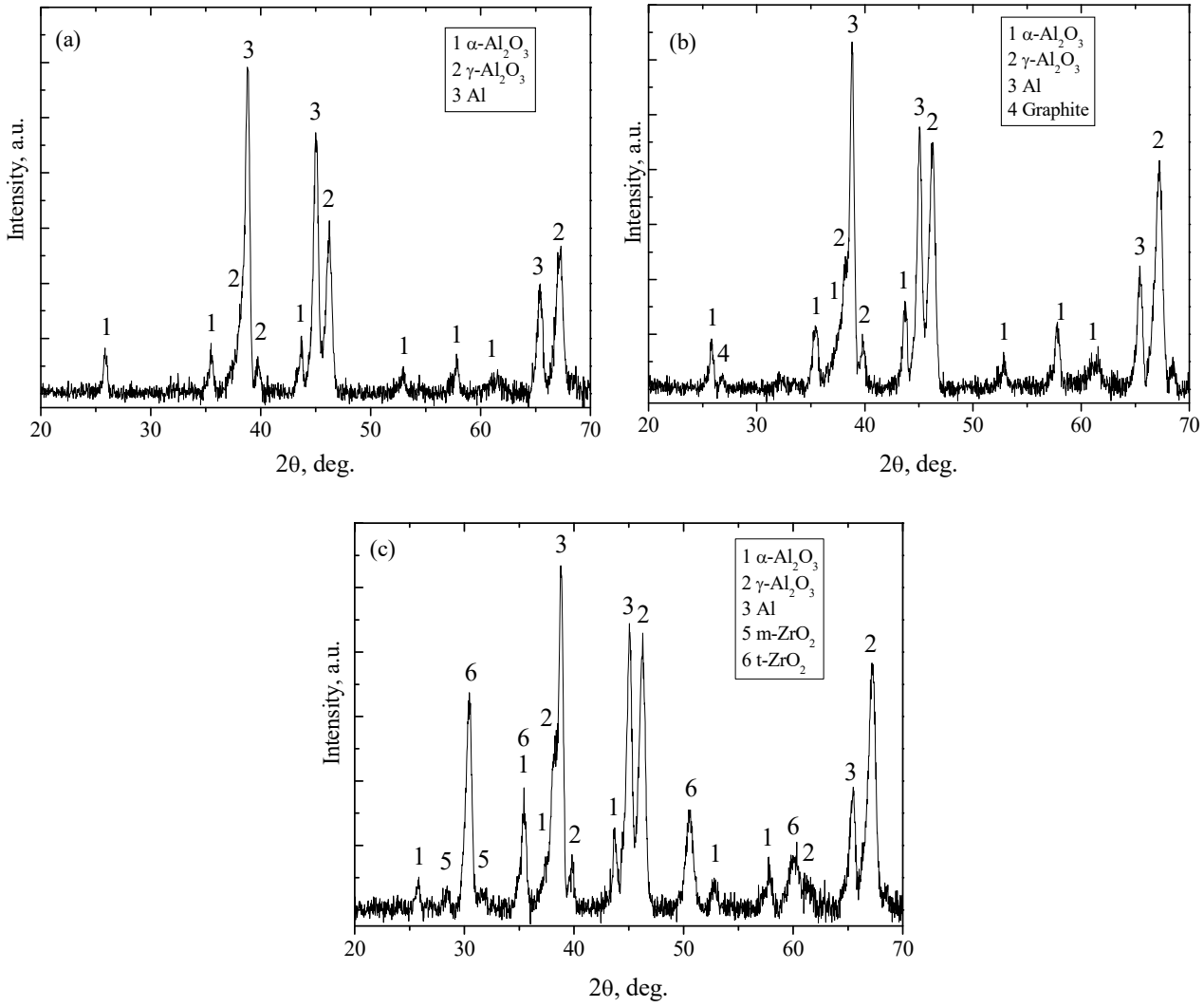

Figure 6. XRD patterns of Al_2O_3 (**a**), Al_2O_3-graphite (**b**) and Al_2O_3-ZrO_2 (**c**) coatings.

The XRD data analysis of the coatings indicated that the graphite or zirconia additives slightly changed the phase structure of the composite coatings. The addition of graphite slightly enhanced the alpha-alumina phase content from 23.7% to 25.1%. Meanwhile, the ZrO_2 powders reduced the alpha-alumina phase amount down to 21.7% in the coating. It was observed that the hardness of Al_2O_3 coatings is enhanced with the increase in the α-Al_2O_3 phase [23]. The data calculated using Equation (2) indicated that the monoclinic ZrO_2 phase content in the Al_2O_3-ZrO_2 coatings was ~17.7%. The amount of m-ZrO_2 phase in the initial ZrO_2-8%Y_2O_3 feedstock powders was ~27.1% [36]. The reduction in the amount of monoclinic ZrO_2 phase is due to the melting of the feedstock powders in the plasma jet. The phase transition occurs when the semi-melted or fully melted ZrO_2 particles reach the surface, stick and finally solidify on the steel substrate [13].

The SEM images and elemental composition measurements were performed after the tribological tests. The deep and wide grooves with sharp edges appeared on the steel roll after tribological tests (Figures 7 and 8), whereas the grooves that formed on the steel plate were deeper and wider and the surface showed many metal chips and areas of peeling (Figures 7 and 9). Wear particles from micrometer to tens of micrometers in size and wear debris in the wear scar could be identified on the surfaces of steel roll and steel plate as debris occurring during dry sliding tests. The formation of deep and sharp grooves on the steel surfaces indicates that in the case of dry sliding, the high friction and rapid wear of the metal surfaces have occurred. These scratches and grooves are generated primarily by the steel asperities, and secondly by the debris detached from the steel roll sample or steel plate, producing a three-body abrasion to some extent. The elemental composition on the wear surface of the steel roll consisted of iron (98.2 wt.%), oxygen (0.5 wt.%) and manganese (1.3 wt.%) with a low number of other materials. The elemental composition at the wear scars of the steel plate was composed of 98.0 wt.% iron, 0.76 wt.% aluminum, 0.9 wt.% oxygen and 1.2 wt.% manganese.

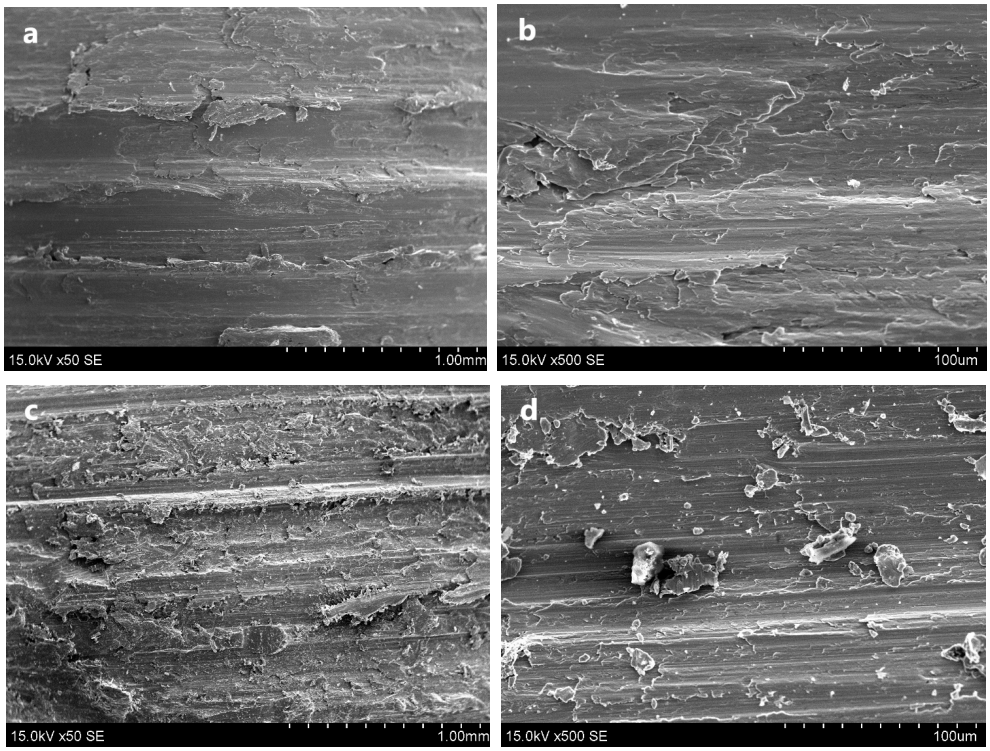

Figure 7. Surface images of steel roll (**a**,**b**) and plate (**c**,**d**) after tribological tests.

The wear scar images of friction pair of the Al_2O_3 coating–steel plate are given in Figure 10. It was obtained that an uneven wear of the Al_2O_3 coating occurred. The coating wears off unevenly over the entire surface, so that in one place, the coating layer remains, while in another place, it is almost completely worn off and a smooth steel surface is visible (Figure 10a,b). Wear scars could be up to 0.5–1.5 mm wide, where Al_2O_3 coatings still remained or were not completely delaminated or removed (Figure 10a). Meanwhile, the micro-sized grooves appeared on the surface of the steel plate. The sliding direction can be easily identified from the grooves that appeared on the worn scars (Figure 10d).

The EDX mapping images of the Al_2O_3 coating were performed at the wear scar zones where the coating was only partly delaminated (Figure 11). The amount of Al varied from 48.3 wt.% to 50.1 wt.%. The oxygen content was ~29.0 $\pm$ 0.5 wt.%. The amount of iron on the less-affected wear scar areas varied from 18.4 to 19.3 wt.%.

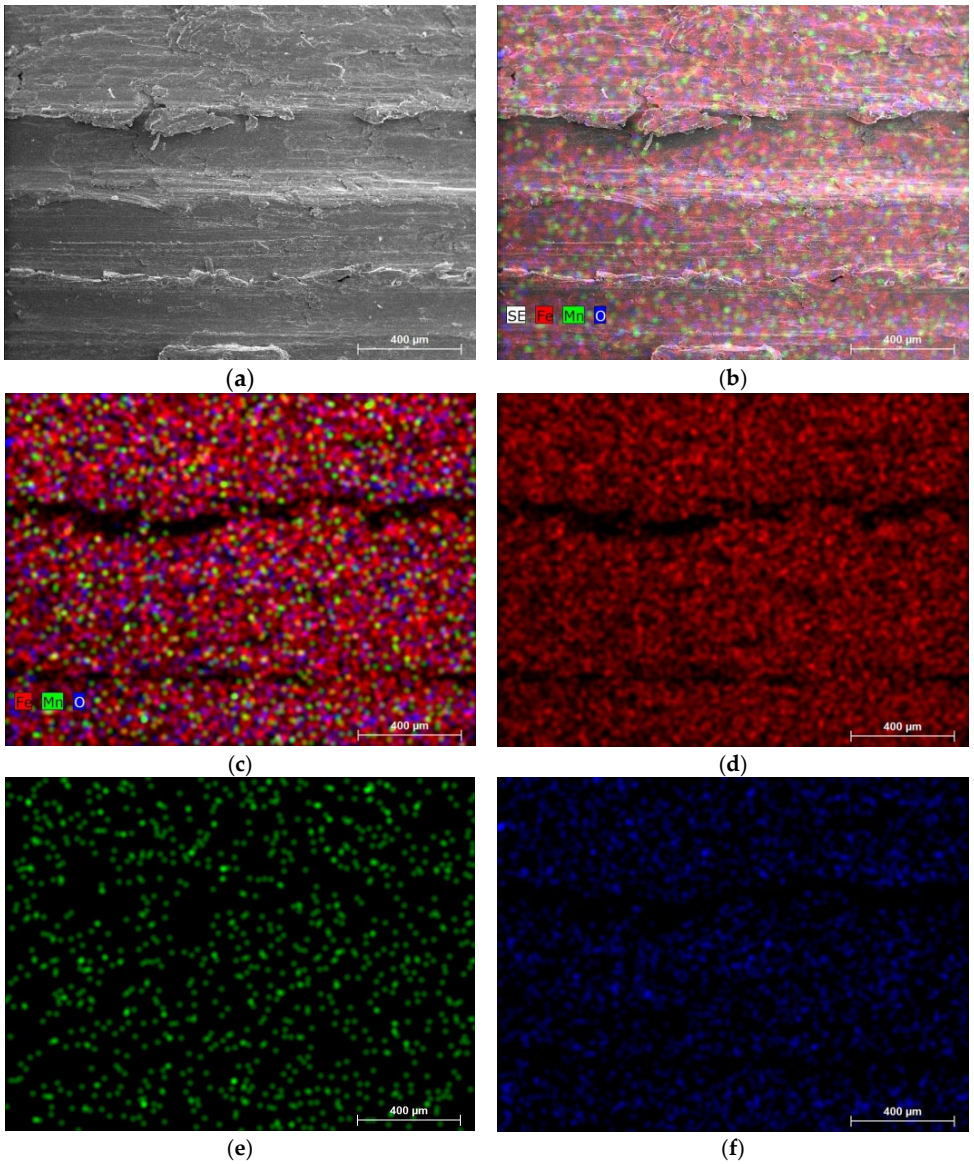

Figure 8. SEM (**a**) and elemental mapping images (**b**–**f**) from the wear scars of steel roll: (**d**) iron, (**e**) manganese and (**f**) oxygen.

A high amount of coating materials was obtained on the wear scar of the steel plate (Figure 12). The surface was fully covered by the aluminum at wear zone and the concentration of the Al varied from 21.2 wt.% to 32.8 wt.% (Figure 12). The amount of oxygen changed from 7.2 to 13.4 wt.%. Traces of carbon and manganese could also be found on the surface (Figure 12b,c). A high content of aluminum indicates that intensive abrasion occurred, leading to the partial delamination of the coating. The delaminated Al_2O_3 parts and fragments are involved in the contact zone and are crushed and smashed during dry sliding tests. As a result, the counterpart steel plate is covered with aluminum oxide.

The worn surfaces of the Al_2O_3-graphite coating and steel plate, and the Al_2O_3-ZrO_2 coating are presented in Figures 13 and 14, respectively. The surface of Al_2O_3-graphite coating becomes smoother, with flat patches and abraded areas (Figure 13a,b). The EDX mapping images indicated that the flat areas are covered by iron (Figure 15). The scratch in the wear trajectory of the Al_2O_3-graphite coating is very narrow, indicating that only a minor removal of the coating occurred (Figure 13b). The wear debris particles randomly distributed on the steel plate could be obtained (Figure 13d). The steel plate surface is quite smooth with grooves and longitudinal strips appearing in the direction of the sliding. As

the hardness of the steel is lower compared to the ceramic coating, iron is transferred to the surface of the coating.

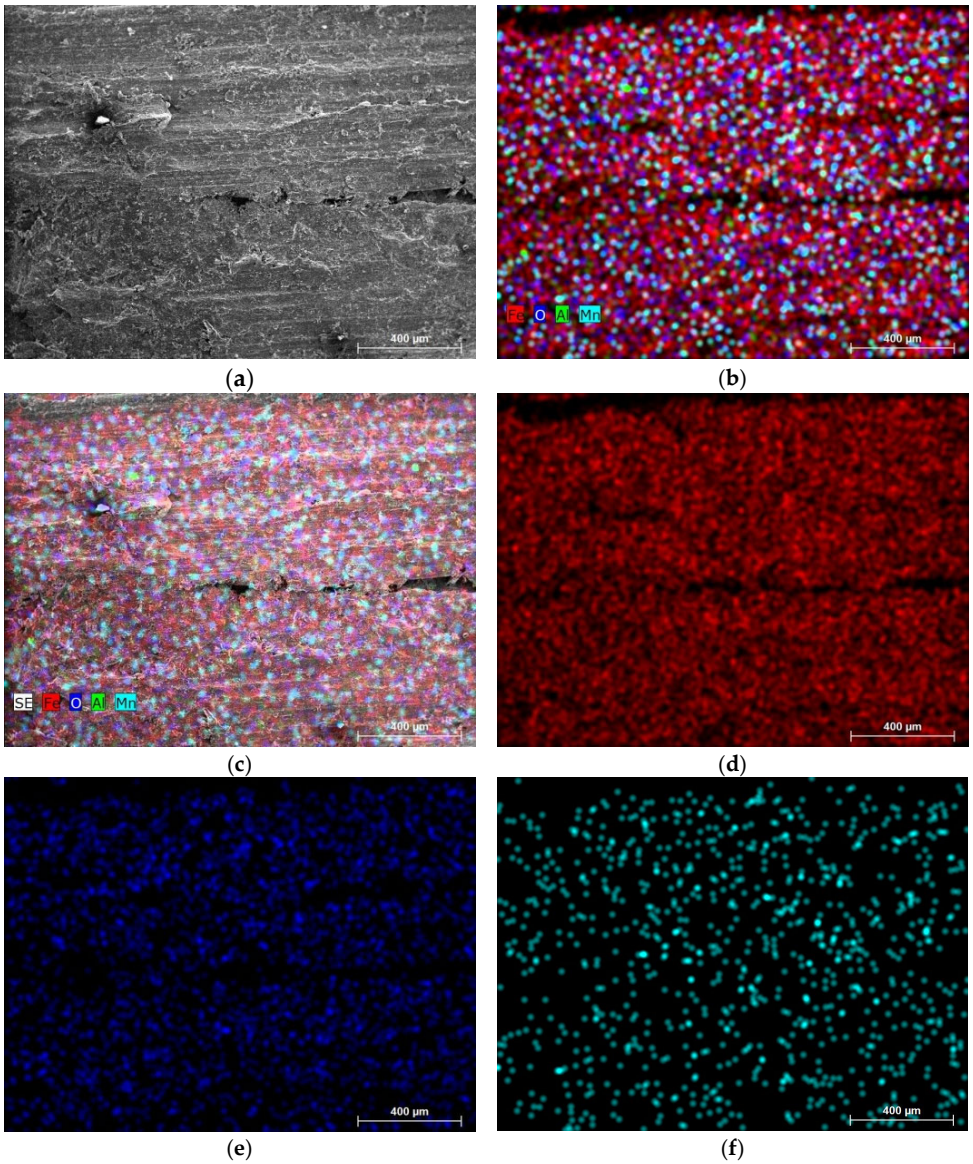

Figure 9. SEM (**a**) and element mapping images of steel plate after tribological test: (**b**,**c**) all elements, (**d**) iron, (**e**) oxygen and (**f**) manganese.

The distribution of oxygen, aluminum, graphite and iron on the surface of wear scars of the Al_2O_3-graphite coating is presented in Figure 15. The EDX mapping images indicated that the alumina and graphite feedstock powders were homogenously spread all over the surface.

The distribution of the elements in the worn areas of the alumina-graphite-and-steel-plate pair are shown in Figures 15 and 16. The co-existence of high concentrations of Fe on the alumina-graphite wear scar was obtained (Figure 15f). Fe-rich zones at the contact area of the ceramic coating are due to a mutual metal material transfer from the counter surface during dry sliding test. The iron-containing zones were distributed quite homogenously in all contact areas of sliding parts. The EDX data indicated that the amount of iron on the wear scar zones varied from 12.7 wt.% to 19.4 wt.%. The concentration of the carbon in the wear scar areas varied from 3.3 to 4.1 wt.% (Figure 15e). The amount of Al on the coating surface varied from 40.0 wt.% to 41.5 wt.%, while the oxygen concentration changed from 38.3 to 41.1 wt.%. The increase in the carbon in the wear scar areas indicates that the

lubricative layer formed at the sliding area. A low amount of aluminum (0.8 wt.%) and carbon (from 1.5 to 3.7 wt.%) was obtained on the wear scars of the steel plate (Figure 16). Both aluminum and carbon were evenly distributed over all areas of the wear scars of the steel plate (Figure 16c,e). This is evidence that the material transfer from the ceramic coating to the steel plate occurred. Additionally, a slight oxidation of the steel surface at the contact zone was induced. The concentration of the oxygen was ~4.3 wt.%.

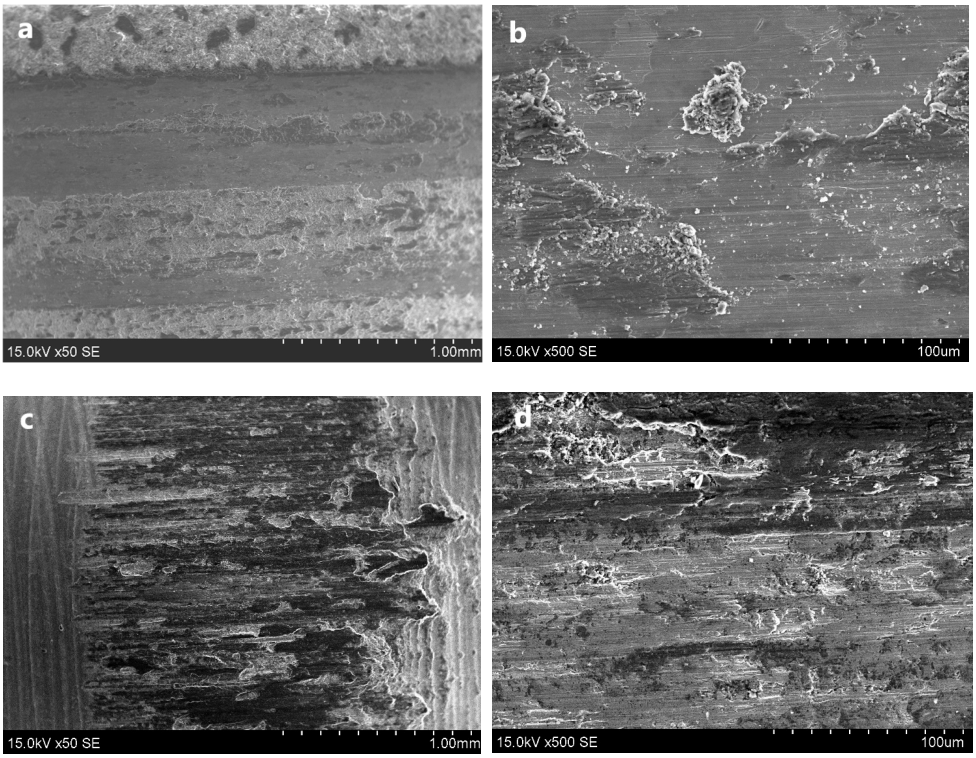

Figure 10. Surface images of Al_2O_3 coating (**a**,**b**) and steel plate (**c**,**d**) after tribological tests.

The EDX data showed that the concentration of iron in the wear scar zones of the Al_2O_3-ZrO_2 coating varied from 20.3 wt.% to 26.5 wt.% (Figure 17). The concentration of the oxygen in the wear scar areas varied from 36.7 to 40.3 wt.%. The concentration of Al was from 32.5 to 34.2 wt.%. The amount of Zr ranged from 2.5 to 3.5 wt.%. Additionally, a low amount (up to 0.5 wt.%) of Mn and carbon was obtained in the wear scar areas.

The wear scar areas of the steel plate after the tribological tests with Al_2O_3-zirconia coating were very similar to those of the Al_2O_3-graphite coating. A low amount of aluminum (up to 1.0 wt.%) and an increase in the oxygen concentration was found on the wear scars of the steel plate. This is evidence of the material transfer from the Al_2O_3-zirconia coating to the steel plate. Additionally, the oxide content on the steel plate surface was enhanced due to the increase in the temperature at the contact zone, which stipulated the formation of the metal-oxidized layer.

The variation in the friction coefficient of coatings versus sliding distance is given in Figure 18. The friction coefficient of the steel sample varies unevenly, as a result of which high fluctuations of the friction coefficient were obtained (Figure 18a). In the case of dry sliding, the steel surface is not protected by the coating, and therefore, the friction coefficient after ~250 m, from a stable value of ~0.11, starts to increase sharply and decreases in the range of 0.1–0.4 due to the unevenly distributed load. The appearance of steel microparticles in the contact zone and an increase in the surface roughness of the steel roll and steel plate are observed. The rapid increase in the friction coefficient fluctuations was observed when the sliding distance became higher than 550 m. Such variation in the friction coefficient indicates a severe abrasive wear failure [2]. The friction coefficient of Al_2O_3 coatings varied from 0.22 to 0.3, when the sliding distance was in the range of 50–450 m. The appearance of

the sharp peaks at a sliding distance of ~470 m is an indication of the high abrasive wear, which could have happened because of the partial delamination of the Al_2O_3 coating under dry sliding. The partial cracking and peeling of the Al_2O_3 coating during the dry sliding test at a distance higher than 500 m was confirmed by analyzing the wear track images (Figures 10 and 11). The temperature at the contact zone was ~25 °C, when the sliding distance was increased from 100 m to 450 m.

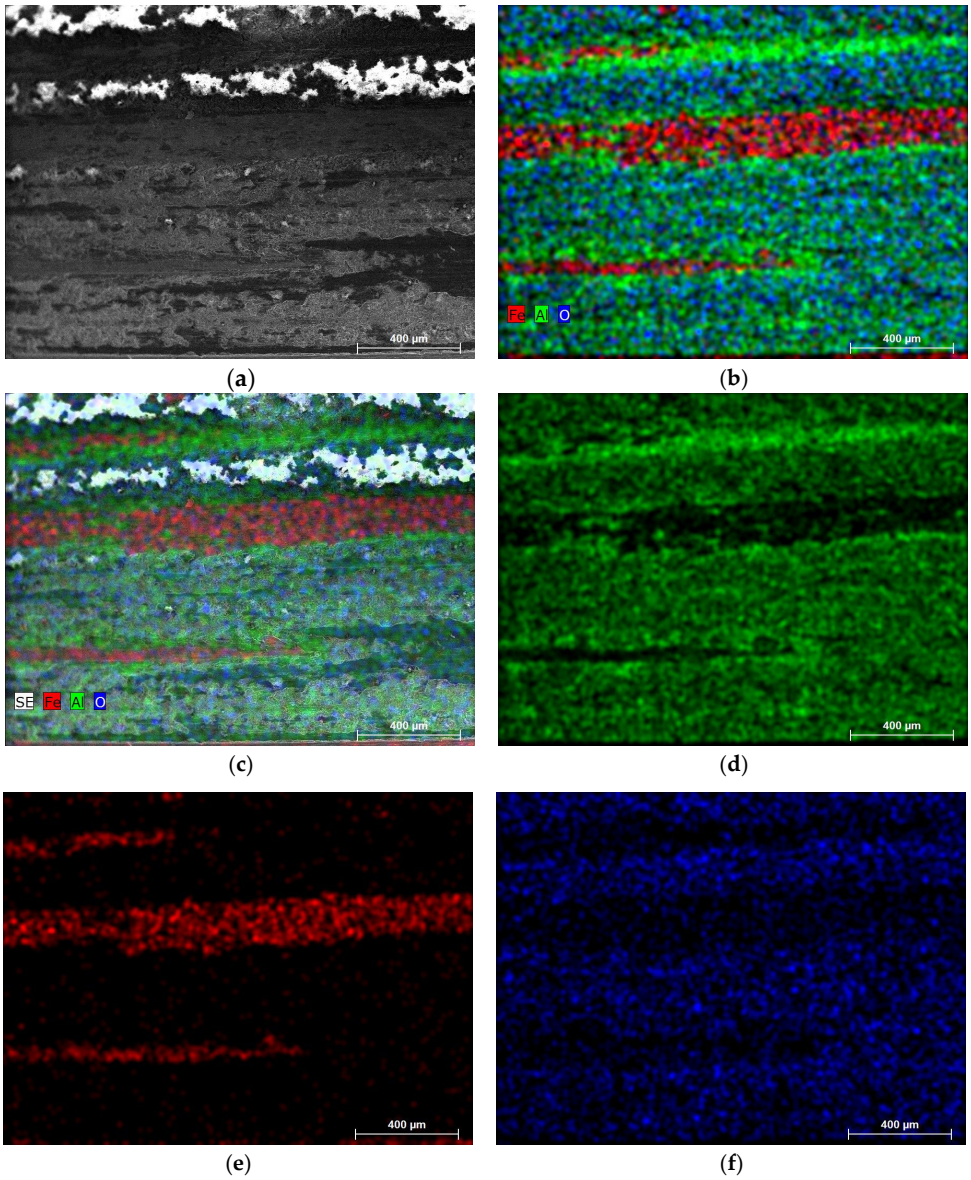

(**a**) (**b**) (**c**) (**d**) (**e**) (**f**)

Figure 11. SEM (**a**) and element mapping images of Al_2O_3 coating of wear scars: (**b**,**c**) all elements, (**d**) aluminum, (**e**) iron and (**f**) oxygen.

A completely different behavior of the friction coefficient versus sliding distance was obtained when graphite and zirconia were added into the alumina feedstock powders. The friction coefficient of the Al_2O_3-graphite coating was constantly increasing from 0.1 up to 0.35 with the rise in sliding distance from 100 m up to 1300 m (Figure 18b). This led to the gradual increase in the temperature from 21 °C up to 32 °C. A similar variation of the friction coefficient was obtained for the Al_2O_3-ZrO_2 coating. The main difference was that the friction coefficient of the Al_2O_3-ZrO_2 was slightly higher (~0.02–0.025) at a distance range of 300–1300 m compared to the friction coefficient of Al_2O_3-graphite coating (Figure 18b). The gradual increase in the temperature from 20 °C up to 33 °C was observed

for the Al_2O_3-ZrO_2 coating surface during the dry sliding friction tests. The continuous increase in friction coefficient is due to the removal of the coating, the formation of an iron layer on the coatings and counterbody wear track created by the reattachment of wear debris [37]. The friction test of Al_2O_3-graphite coating was discontinued because the coating was able to withstand the applied load very well with only minor wear. This happened because the graphite in the coating, due to its layered structure, acts as a lubricant during dry friction and forms a protective layer between the coating and the steel plate [17,22,26]. Despite the fact that the friction coefficient of the Al_2O_3-ZrO_2 coating was the highest, only a minor wear was observed on the coating surface (Figures 14 and 17).

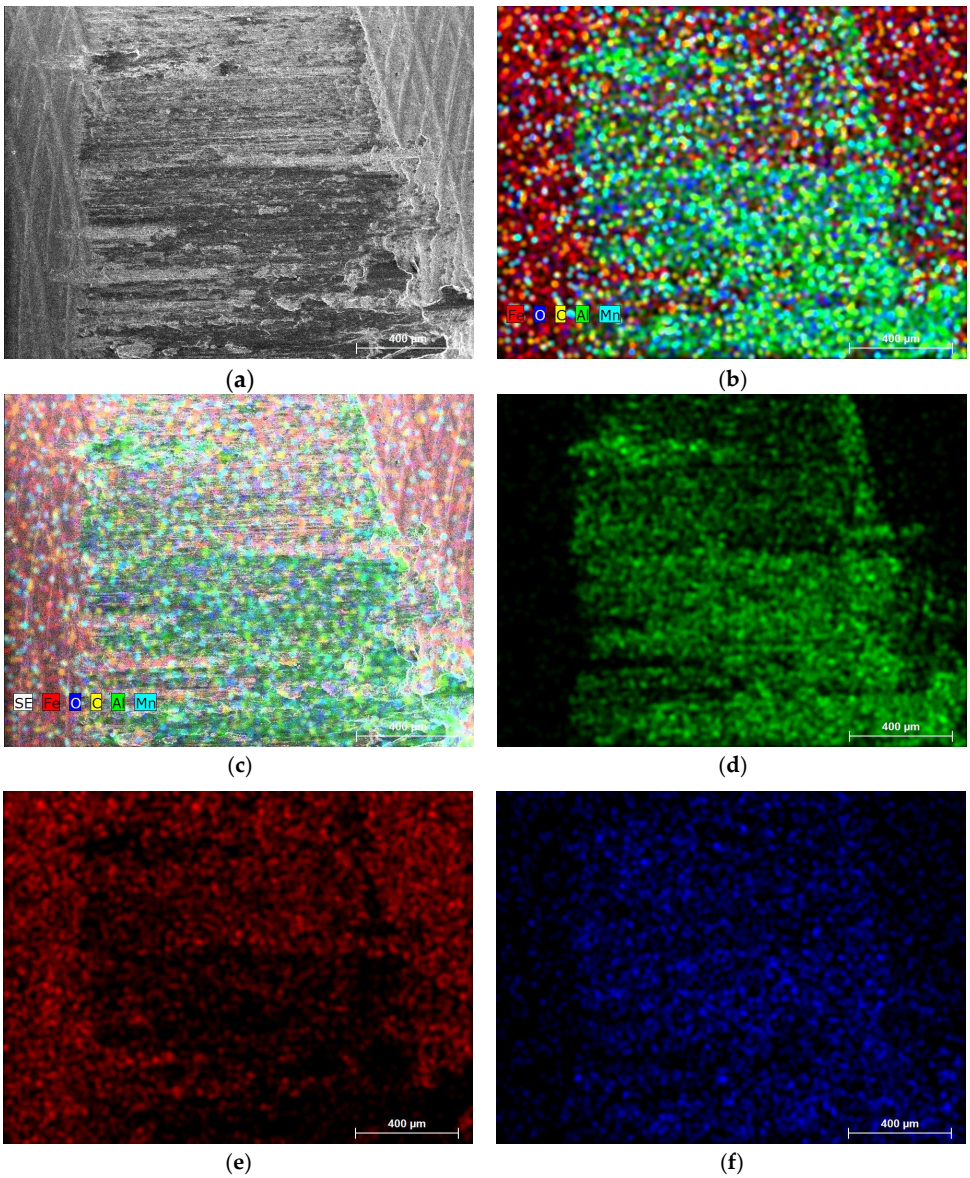

Figure 12. SEM (**a**) and elemental mapping images (**b**–**f**) from wear scars of steel plate: (**d**) aluminum, (**e**) iron and (**f**) oxygen.

The weight loss rate of the C45 steel roll and coatings after the tribological tests using a 30 N load was determined. It should be noted that the sliding distance for the friction pair C45 steel roll and steel plate was only 600 m; the first signs of adhesive wear could already be observed at 300 m (the peak of the coefficient of friction) due to the high wear rate of the steel roll and its counterpart, where deep groves were formed and resulted in failure of sliding tests. When the first peaks of the friction coefficient appeared, a small

amount of wear chips removed from the contact zone could be observed after the friction pair. However, no clear signs of tribocorrosion were observed. The average sliding distance for the alumina–steel plate pair was ~450 m. The partial delamination and cracking of the alumina coatings started and resulted in the failure of the tribological tests. As it can be seen, by adding graphite or zirconia to the alumina coating, the wear resistance of the coatings was improved. The surface of the Al_2O_3-graphite and Al_2O_3-ZrO_2 coatings was only slightly worn out after a sliding distance of 1300 m (Figures 13 and 14).

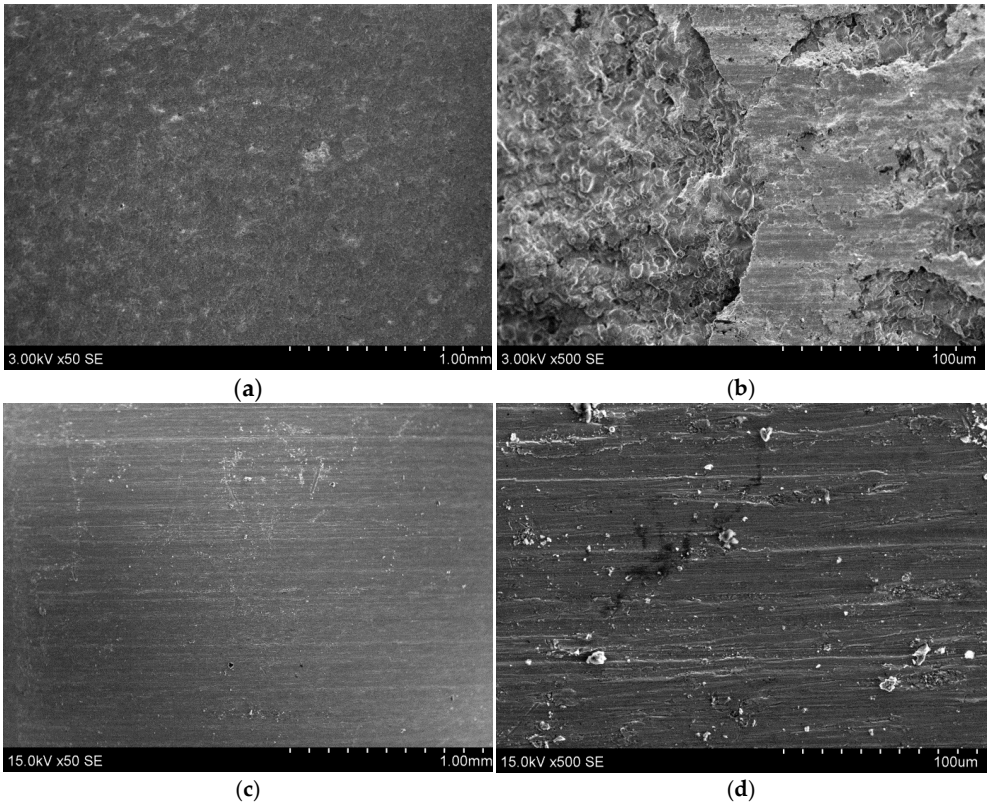

Figure 13. Surface images of Al_2O_3-graphite coating (**a**,**b**) and steel plate (**c**,**d**) after tribological tests.

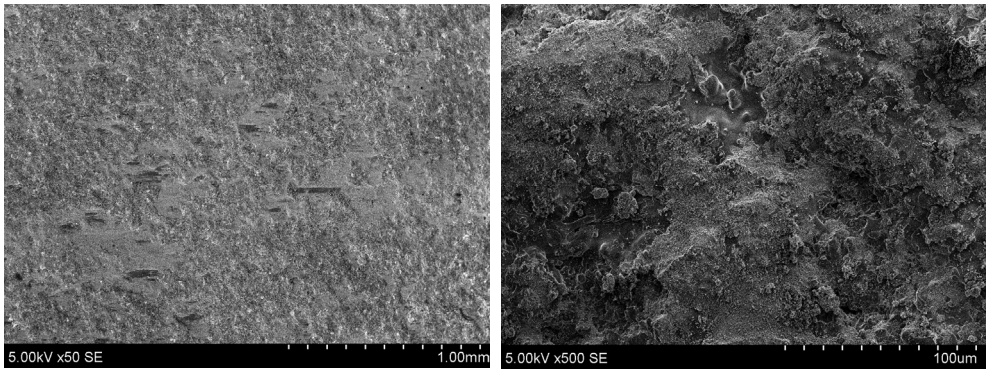

Figure 14. Surface images of the wear tracks of Al_2O_3-ZrO_2 coating.

The mass loss rate of the coatings and steel plates were determined after the tribological tests (Table 2). The average mass loss rates of the steel roll and plate were 8.84×10^{-4} g/s and 1.50×10^{-4} g/s, respectively. Even though the alumina coating was partially delaminated, its wear rate was 2.42×10^{-4} g/s. While the wear rate of the counterpart steel was ~0.35×10^{-4} g/s. The much lower wear rate of 4.2×10^{-6} g/s was observed when the Al_2O_3-ZrO_2 coating was used. The wear rate of the Al_2O_3-graphite coating was 3.3×10^{-6} g/s. The wear rates of the steel plates,

when Al_2O_3-ZrO_2 and Al_2O_3-graphite coatings were used were 22.3 × 10^{-6} g/s and 39.3 × 10^{-6} g/s, respectively.

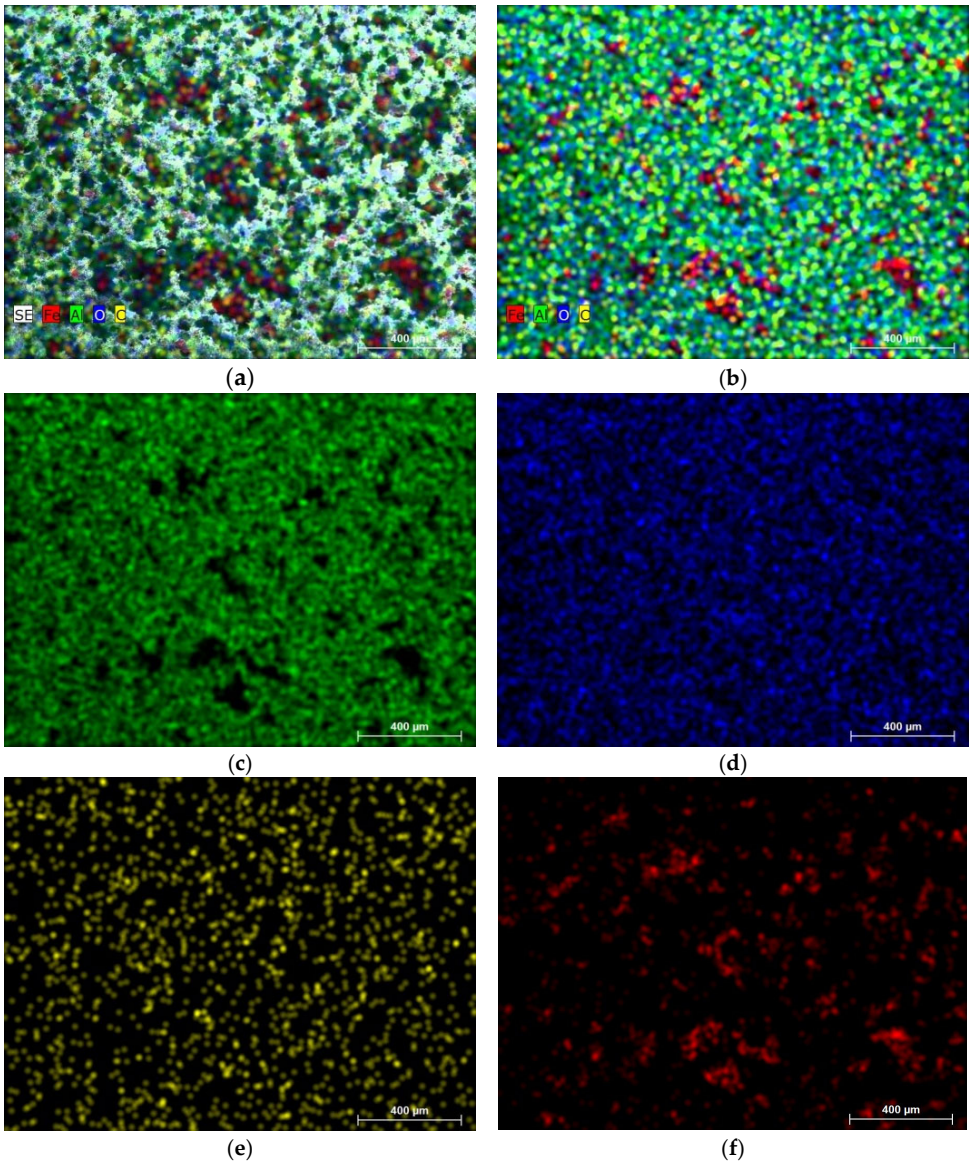

Figure 15. Element mapping images of Al_2O_3-graphite coating after tribological test: (**a**,**b**) all elements, (**c**) aluminum, (**d**) oxygen, (**e**) graphite and (**f**) iron.

Table 2. Mass loss rates of the coatings and steel plates.

Materials on Roll	Mass Loss Rate, g/s	Steel Plate Mass Loss Rate, g/s
C45 Steel	8.84 × 10^{-4}	150 × 10^{-6}
Al_2O_3	2.42 × 10^{-4}	35.0 × 10^{-6}
Al_2O_3-graphite	3.3 × 10^{-6}	39.3 × 10^{-6}
Al_2O_3-ZrO_2	4.2 × 10^{-6}	22.3 × 10^{-6}

Brittle fracture and abrasive grooving are the main wear mechanisms observed for the various ceramic coatings under dry sliding conditions [15,23,24,37]. It was found that an initial wear mechanism for the Al_2O_3 coatings or their composites can begin as an adhesive, in which produced micro-sized wear particles adhere to each other or are entrapped, leading to three-body abrasive wear [37]. Furthermore, EDX analysis on the steel plate surface confirmed the presence of low concentrations of

aluminum, carbon or zirconium, indicating material transfer from the graphite- or zirconia-containing composite coating to the steel plate (counter surface). Such material transfer will reduce the wear rates for the steel plate used as a counter surface and the Al_2O_3-graphite coating compared to the alumina-coating-and-steel-plate friction pair [23]. It was demonstrated that the wear volume loss was reduced from ~36 mm^3 to 10 mm^3 with the addition of the graphene nanoparticles in the Al_2O_3 coating [26]. B. Liang et al. [15] observed that the transfer of iron and chromium from a 100C6 steel ball on the surface of Al_2O_3-ZrO_2 coatings was achieved and the formation of such a metallic layer could reduce the wear rate but slightly increase the friction coefficient. Additionally, the Al_2O_3-ZrO_2 coatings with lower porosity, higher adhesion strength and microhardness demonstrated better tribological properties [15]. The iron-containing areas were detected on the worn surface of the coatings, indicating that the transfer of Fe from the counterpart plate to the coating surface occurred (Figures 15f and 17f). This could be one of the reasons for the slight increase in the friction coefficient of the Al_2O_3-graphite and Al_2O_3-ZrO_2 coatings versus sliding distance (Figure 18b).

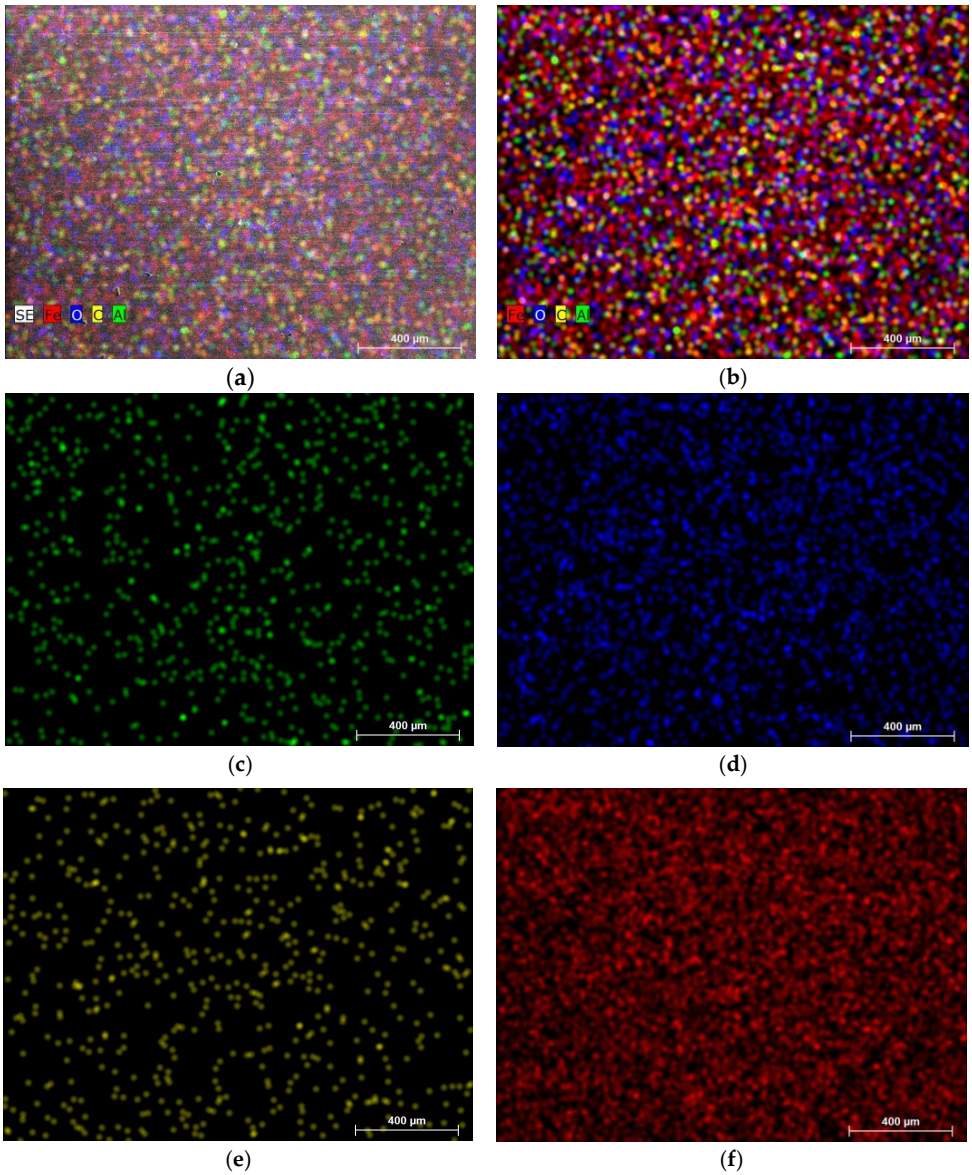

Figure 16. Element mapping images of steel plate (used in pair with Al_2O_3-graphite coating) wear scars: (**a**,**b**) all elements, (**c**) aluminum, (**d**) oxygen, (**e**) graphite and (**f**) iron.

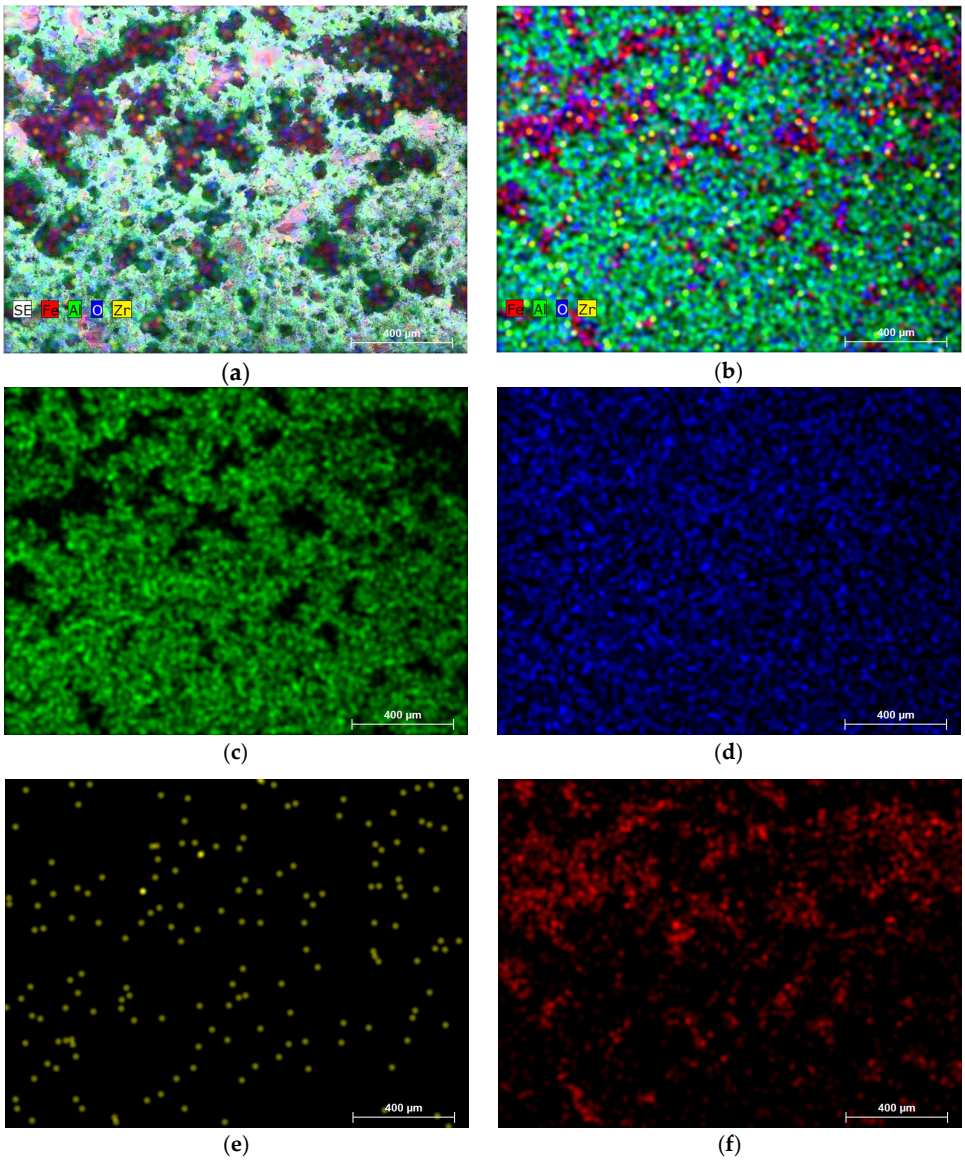

Figure 17. Element mapping images of Al_2O_3-ZrO_2 coating after tribological test: (**a**,**b**) all elements, (**c**) aluminum, (**d**) oxygen, (**e**) zirconium and (**f**) iron.

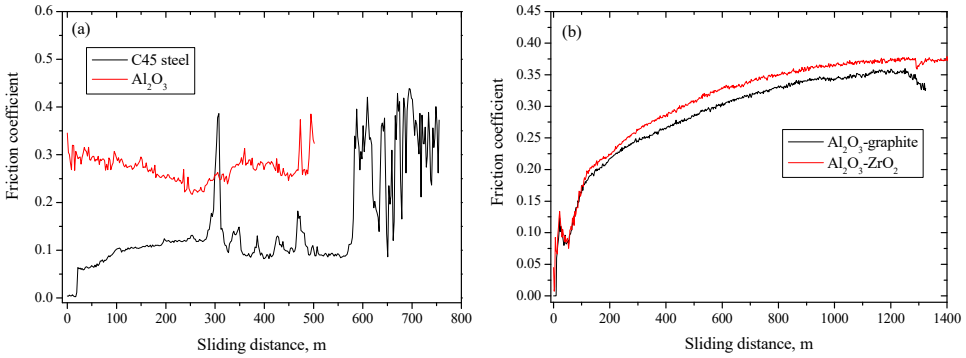

Figure 18. Variation in friction coefficient of the steel and deposited coatings versus sliding distance.

Elemental maps presented in Figures 15–17 proved that the tribofilm contains iron, carbon or zirconium, aluminum and oxygen. It indicates that the tribolayer from the accumulation of plastically deformed debris from Al_2O_3-graphite or Al_2O_3-ZrO_2 coating and steel plate was formed on the worn surfaces. The compactness and integrity of the

formed transferred tribofilm will reduce the wear rate of the coating as they prevent direct contact between Al_2O_3-graphite or Al_2O_3-ZrO_2 coating and their counterpart. It was demonstrated that the addition of various carbon materials (graphene, graphene oxide) reduced the friction coefficient of Al_2O_3 or Al_2O_3 composite coatings [17,18,22–25,28]. The main reason for the reduction in friction coefficient is the formation of a self-lubricative layer in the sliding contact zone.

The obtained tribological results indicated that the addition of graphite or zirconia into alumina coatings improved the tribological behavior and wear resistance of the coatings. It was demonstrated that the addition of ZrO_2 into Al_2O_3 led to a greater toughness of the composite coatings [11]. The melting temperature of the ZrO_2 is ~2680 °C, while the melting temperature of the Al_2O_3 is lower (2050 °C). The temperature required to fully melt the Al_2O_3-ZrO_2 powders would be higher than the one for Al_2O_3 feedstock powders. Thus, the porosity of the Al_2O_3-ZrO_2 coating would probably be slightly higher compared to Al_2O_3 coatings. However, the existence of the pores in the coatings could have a positive effect on accumulating the propagation of microcracks under high loads [2,11]. The addition of the graphite probably resulted in a lower porosity value of the alumina-graphite coatings [17,26,27]. Several studies demonstrated [24–26] that the addition of low amounts of graphene reduced the porosity of ceramic coatings. The plasma jet temperature in the powder injection place was similar to or higher than the graphite sublimation temperature. The additional heat released as part of the graphite will sublimate in the plasma jet and will improve the melting degree of the alumina particles. It will result in better adhesion between the individual splats during the solidification of the feedstock particles on the surface and result in improved tribological behavior. The adhesion of the alumina coatings was improved with the addition of graphene oxide. It was demonstrated that due to the higher thermal conductivity and a higher surface area of graphene oxide, a better melting of previously solidified layers will be stipulated, and it will enhance the bonding between lamellar interfaces and result in lower porosity values [26]. It was obtained that Ni-Al_2O_3/graphite composite coatings with a low amount of graphite demonstrated similar hardness and better tribological properties. Thus, the introduction of low amounts of graphite (2.3 wt.%) will maintain its similar hardness to Al_2O_3 coatings. The hard Al_2O_3 matrix will hold the softer graphite particles without loosening debris or fragments to suppress further severe wearing of the coating [38]. A similar effect is expected to be provided on the alumina coating when graphite powder is used as an additive.

4. Conclusions

Alumina, alumina-graphite and alumina-zirconia coatings were deposited on a C45 steel roll by atmospheric plasma spraying. The addition of graphite slightly reduced (up to 8%) the average surface roughness of the alumina coating. The concentration of the graphite in the alumina-graphite coatings was only 2.3 wt.%. The Al_2O_3 and Al_2O_3-graphite coatings were composed of α-Al_2O_3 and γ-Al_2O_3 phases, with a low amount of crystalline graphite when the graphite additive was used. The alumina-zirconia coatings consisted of α-Al_2O_3, γ-Al_2O_3, t-ZrO_2 and m-ZrO_2 phases. It was demonstrated that the graphite additive slightly enhanced the amount of α-Al_2O_3 phase, while the zirconia additive reduced the α-Al_2O_3 in the coatings. The results indicated that the monoclinic ZrO_2 phase content in the Al_2O_3-ZrO_2 coatings was ~17.7%. The lowest friction coefficient of ~0.1 was obtained for the steel roll, but due to the high abrasiveness and wear of the steel parts, the duration of the tribological test was limited to 600 m. The addition of graphite or zirconia drastically enhanced the wear resistance of the alumina coatings under dry sliding conditions when a 30 N load was used. It was obtained that the mass loss rate for the Al_2O_3-graphite and Al_2O_3-zirconia coatings was only 3.3×10^{-6} g/s and 4.2×10^{-6} g/s, respectively. The mass loss rate of the Al_2O_3-graphite and Al_2O_3-zirconia coatings was more than two orders of magnitude lower compared to alumina coatings or steel. The Al_2O_3-graphite and Al_2O_3-zirconia coatings were only slightly worn out due to the formation of the lubricative layer at the coating-steel contact area. The performed investigation showed that zirconia

and graphite additives are suitable materials to improve the tribological properties of alumina coatings in order to achieve a longer lifetime of the steel roll under dry sliding conditions. The future trend could be related to the investigations on the effect of additive concentrations (graphite, ZrO_2 or Cr_2O_3) on the tribological properties of Al_2O_3 coatings.

Author Contributions: Conceptualization, Ž.K., R.K. and L.M.; methodology, K.R., A.Ž. and L.M.; software, A.Ž., K.R., M.A. and R.K.; validation, K.R., A.Ž. and L.M.; formal analysis, K.R., A.Ž. and L.M.; investigation, K.R., Ž.K., R.K., M.A., A.Ž. and L.M.; resources, M.A. and L.M.; data curation, K.R., Ž.K. and L.M.; writing—original draft preparation, L.M.; writing—review and editing, A.Ž. and L.M.; visualization, Ž.K., K.R., A.Ž. and L.M.; supervision, L.M. All authors have read and agreed to the published version of the manuscript.

Funding: This research received no external funding.

Institutional Review Board Statement: Not applicable.

Informed Consent Statement: Not applicable.

Data Availability Statement: Data is contained within the article.

Conflicts of Interest: The authors declare no conflicts of interest.

References

1. Edward, J.; Gildersleeve, V.; Vaben, R. Thermally Sprayed Functional Coatings and Multilayers: A Selection of Historical Applications and Potential Pathways for Future Innovation. *J. Therm. Spray. Technol.* **2023**, *32*, 778–817. [CrossRef]
2. Aghajani, H.; Valefi, Z.; Zamani, P. Phase composition, microstructure, mechanical properties, and wear performance of nanostructured Al_2O_3 and Al_2O_3-Y_2O_3 coatings deposited by plasma spraying. *Appl. Surf. Sci.* **2022**, *585*, 152754. [CrossRef]
3. Deng, W.; Li, S.; Hou, G.; Lia, X.; Zhao, X.; An, Y.; Zhoa, H.; Chen, J. Comparative study on wear behaviour of plasma sprayed Al_2O_3 coatings sliding against different counterparts. *Ceram. Int.* **2017**, *43*, 6976–6986. [CrossRef]
4. Misra, V.; Chakravarthy, Y.; Khare, N.; Singh, K.; Ghoru, S. Strongly adherent Al2O3 coating on SS 316L: Optimization of plasma spray parameters and investigation of unique wear resistance behaviour under air and nitrogen environment. *Ceram. Int.* **2020**, *46*, 8658–8668. [CrossRef]
5. Heimann, R.B. *Plasma Spray Coating Principles and Applications*; Wiley-VCH: Weinheim, Germany, 2008.
6. Franco, D.; Ageorges, H.; López, E.; Vargas, F. Tribological performance at high temperatures of alumina coatings applied by plasma spraying process onto a refractory material. *Surf. Coat. Technol.* **2019**, *371*, 276–286. [CrossRef]
7. Kang, J.J.; Xu, B.S.; Wang, H.D.; Wang, C.B. Influence of spraying parameters on the microstructure and properties of plasma-sprayed Al2O3/40%TiO2 coating. *Phys. Procedia* **2013**, *50*, 169–176. [CrossRef]
8. Kwon, H.; Yoo, Y.; Park, Y.; Nam, U.; Byon, E. Effect of TiO_2 on mechanical and thermal properties of Al2O3-based coating via atmospheric plasma spraying. *J. Asian Ceram. Soc.* **2023**, *2*, 282–290. [CrossRef]
9. Younes, R.; Bradai, M.; Sadeddine, A.; Mouadj, Y.; Bilek, A.; Benabbas, A. Effect of TiO_2 and ZrO_2 reinforcements on properties of Al_2O_3 coatings fabricated by thermal flame spraying. *Trans. Nonferr. Met. Soc. China* **2016**, *26*, 1345–1352. [CrossRef]
10. Bannier, M.; Vicent, E.; Rayón, R.; Benavente, M.D.; Salvador, E.; Sánchez, E. Effect of TiO_2 addition on the microstructure and nanomechanical properties of Al_2O_3 Suspension Plasma Sprayed coatings. *Appl. Surf. Sci.* **2014**, *316*, 141–146. [CrossRef]
11. Mehar, S.; Sapate, S. Contact severity maps for plasma sprayed YSZ modified Al_2O_3-3% TiO_2 coatings. *Ceram. Int.* **2024**, *50*, 13003–13013. [CrossRef]
12. Chen, Y.; Yang, Y.; Chu, Z.; Chen, X.; Wang, L.; Liu, Z.; Dong, Y.; Yan, D.; Zhang, J.; Kang, Z. Microstructure and properties of Al_2O_3 -ZrO_2 composite coatings prepared by air plasma spraying. *Appl. Surf. Sci.* **2018**, *431*, 93–100. [CrossRef]
13. Kiilakoski, J.; Musalek, R.; Luka, F.; Koivuluoto, H.; Vuoristo, P. Evaluating the toughness of APS and HVOF-sprayed Al_2O_3-ZrO_2-coatings by in-situ- and macroscopic bending. *J. Eur. Ceram.* **2018**, *38*, 1908–1918. [CrossRef]
14. Tingaud, O.; Bertrand, P.; Bertrand, G. Microstructure and tribological behavior of suspension plasma sprayed Al_2O_3 and Al_2O_3–YSZ composite coatings. *Surf. Coat. Technol.* **2010**, *205*, 1004–1008. [CrossRef]
15. Liang, B.; Zhang, G.; Liao, H.; Coddet, C.; Ding, C. Friction and wear behaviour of ZrO_2–Al_2O_3 composite coatings deposited by air plasma spraying: Correlation with physical and mechanical properties. *Surf. Coat. Technol.* **2009**, *203*, 3235–3242. [CrossRef]
16. Wang, Y.-W.; Wang, X.-L.; Wang, X.-Y.; Yang, Y.; Zhang, C.; Sun, W.; Ma, Y.; Cui, Y.; Wang, L.; Dong, Y. Effect of CeO_2 on the Microstructure and Properties of Plasma-Sprayed Al_2O_3-ZrO_2 Ceramic Coatings. *J. Mater. Eng. Perform.* **2020**, *29*, 6390–6401. [CrossRef]
17. Marcinauskas, L.; Mathew, J.S.; Milieška, M.; Aikas, M.; Kalin, M. Influence of graphite content on the tribological properties of plasma sprayed alumina-graphite coatings. *Surf. Interfaces* **2023**, *38*, 102763. [CrossRef]
18. Marcinauskas, L.; Mathew, J.S.; Milieška, M.; Aikas, M.; Kalin, M. Effect of graphite concentration on the tribological performance of alumina coatings. *J. Alloys Compd.* **2020**, *827*, 154135. [CrossRef]

19. Marcinauskas, L.; Mathew, J.S.; Milieška, M.; Thanigachalam, B.; Kupec, A.; Česnavičius, R.; Kėželis, R.; Kalin, M. Microstructure and tribological properties of plasma sprayed alumina and alumina-graphite coatings. *Surf. Coat. Technol.* **2018**, *350*, 401–409. [CrossRef]
20. Mathew, J.S.; Marcinauskas, L.; Kavaliauskas, Ž.; Kėželis, R.; Kalin, M. Effect of Spraying Power on the Tribological Properties of Alumina and Alumina-Graphite Coatings. *Coatings* **2023**, *13*, 1165. [CrossRef]
21. Habib, K.A.; Cano, D.L.; Serrano-Mira, J.; Rayon, E.; Jose, V.; Nebot, A.; Dosta, S. Tribology behaviour of graphene-modified nanostructured Al2O3/3 % TiO2 coatings under boundary and mixed lubrication conditions. *Wear* **2024**, *548*, 205381. [CrossRef]
22. Mulone, A.; Silva, P.; Yuan, H.; Thånell, K.; Hitchcock, A.; Klement, U. Synchrotron X-ray spectromicroscopy analysis of wear tested graphene-containing alumina coatings. *Carbon.* **2024**, *227*, 119245. [CrossRef]
23. Mahade, S.; Mulone, A.; Bjorklund, S.; Klement, U.; Joshi, S. Incorporation of graphene nano platelets in suspension plasma sprayed alumina coatings for improved tribological properties. *Appl. Surf. Sci.* **2021**, *570*, 151227. [CrossRef]
24. Liu, C.; Sun, J.; Venturi, F.; Romero, A.; Hussain, T. Microstructure and wear performance of alumina/graphene coating on textured Al_2O_3/TiC substrate composites. *J. Eur. Ceram.* **2021**, *41*, 1438–1451. [CrossRef]
25. Murray, J.W.; Ranceb, G.A.; Xua, F.; Hussain, T. Alumina-graphene nanocomposite coatings fabricated by suspension high velocity oxy-fuel thermal spraying for ultra-low-wear. *J. Eur. Ceram. Soc.* **2018**, *38*, 1819–1828. [CrossRef]
26. Priyadershini, S.; Rahman, O.S.A.; Pandey, K.K.; Keshri, A.K. Remarkable improvement in tribological behavior of plasma sprayed carbon nanotube and graphene nanoplatelates hybrid reinforced alumina nanocomposite coating. *Ceram. Int.* **2019**, *45*, 5768–5778. [CrossRef]
27. Li, Y.; Liu, J.; Deng, J.; He, J.; Qin, Y.; Xing, Y.; Yin, F. Fabrication of graphene oxide reinforced plasma sprayed Al_2O_3 coatings. *Ceram. Int.* **2023**, *49*, 1667–1677. [CrossRef]
28. Mohapatra, S.; Dash, T.; Patnaik, T.; Biswa, S. Improvement of hardness and anti-corrosion behavior of mild steel by plasma sprayed coating of Al_2O_3/GO composite. *J. Indian Chem. Soc.* **2023**, *100*, 100996. [CrossRef]
29. Pattnayak, A.; Gupta, A.; Abhijith, N.V.; Kumar, D.; Jain, J.; Chaudhry, V. Development of rGO doped alumina-based wear and corrosion resistant ceramic coatings on steel using HVOF thermal spray. *Ceram. Int.* **2023**, *49*, 17577–17591. [CrossRef]
30. Zhang, Y.; Sun, S.; Zhao, L.; Yang, C.; Wu, L.; Guo, Y.; Ang, A.S.M. Corrosion Behavior of Plasma-Sprayed Al_2O_3-3%TiO_2 Coatings Doped with CeO_2. *J. Therm. Spray Technol.* **2023**, *32*, 290–305. [CrossRef]
31. Brinkienė, K.; Kėželis, R.; Mečius, V. Effect of outlet nozzle design on the YSZ particle in-flight characteristics in plasma jet generated by DC plasma torch. In *Advances in Heat Transfer Engineering*; Begell House: Danbury, CT, USA, 2003; pp. 629–636.
32. Aruna, S.T.; Balaji, N.; Shedthi, J.; Grips, V.K.W. Effect of critical plasma spray parameters on the microstructure, microhardness and wear and corrosion resistance of plasma sprayed alumina coatings. *Surf. Coat. Technol.* **2012**, *208*, 92–100. [CrossRef]
33. Mu, M.; Zhou, X.; Xiao, Q.; Liang, J.; Huo, X. Preparation and tribological properties of self-lubricating TiO2/graphite composite coating on Ti6Al4V alloy. *Appl. Surf. Sci.* **2012**, *258*, 8570–8576. [CrossRef]
34. Dong, H.; Yao, J.T.; Li, J.; Zhou, Y.; Li, Y.B. The sintering behavior of plasma-sprayed YSZ coating over the delamination crack in low temperature environment. *Ceram. Int.* **2018**, *44*, 3326–3332. [CrossRef]
35. Dejang, N.; Limpichaipanit, A.; Watcharapasorn, A.; Wirojanupatump, S.; Niranatlumpong, P.; Jiansirisomboon, S. Fabrication and properties of plasma-sprayed Al_2O_3/ZrO_2 composite coatings. *J. Therm. Spray. Technol.* **2011**, *20*, 259–1268. [CrossRef]
36. Mathew, J.S.; Marcinauskas, L.; Kalin, M.; Kėželis, R.; Kavaliauskas, Ž.; Gecevičius, G.; Čapas, V. Improvement of the Tribological Properties of Alumina Coatings by Zirconia Addition. *Coatings* **2021**, *11*, 991. [CrossRef]
37. Murray, J.W.; Ang, A.S.M.; Pala, Z.; Shaw, E.C.; Hussain, T. Suspension High Velocity Oxy-Fuel (SHVOF)-Sprayed Alumina Coatings: Microstructure, Nanoindentation and Wear. *J. Therm. Spray. Technol.* **2016**, *25*, 1700–1710. [CrossRef]
38. Sun, W.C.; Zhang, P.; Zhao, K.; Tian, M.M.; Wang, Y. Effect of graphite concentration on the friction and wear of Ni–Al_2O_3/graphite composite coatings by a combination of electrophoresis and electrodeposition. *Wear* **2015**, *342–343*, 172–180. [CrossRef]